



## Characterization and Spectroscopic Study of a Heat-Treated and Acid-Leached Halloysite Used in Congo Red Adsorption

Fatiha Bessaha<sup>1\*</sup>, Nouria Mahrez<sup>1</sup>, Souhila Bendenia<sup>1</sup>, Fatima Kasmi<sup>1</sup>, Kheira Marouf-Khelifa<sup>1</sup>,  
 Amine Khelifa<sup>1</sup>

<sup>1</sup>Laboratoire de Structure, Elaboration et Applications des Matériaux Moléculaires (S.E.A.2M.),  
 Département de Chimie, Université de Mostaganem, B.P. 981, R.P., Mostaganem 27000, Algeria

\* Corresponding author's Email: fatiha\_bessaha@yahoo.fr

---

**Abstract:** Algerian halloysite was heated at 600 °C and treated with HCl 5N. The materials were characterized by chemical analysis, TEM, and FT-IR spectroscopy, and used in the elimination of Congo red (CR) from aqueous solution. The effects of contact time and temperature were investigated. The thermal treatment at 600 °C results in the formation of dehydroxylated structure. Acid attack involves an increase in SiO<sub>2</sub> content, due to the leaching of Al ions from octahedral sheet. Thermo-chemical treatment also diminishes the percentage of impurities and maintains the tubular morphology. Kinetic data follow the pseudo-second order model, whilst thermodynamic parameters lead to a not spontaneous and endothermic process. Significant changes occur in the vibrational spectrum of H600-5N (halloysite treated at 600 °C and with HCl 5N), after adsorption of Congo red, with the involvement of amino and sulfoxide groups. The mechanism highlights an outer-sphere surface complexation of SiOH...H<sub>2</sub>O species, i.e., SiOH linked to H<sub>2</sub>O via H-bonds.

**Keywords:** Halloysite, Characterization, Adsorption, FTIR.

---

### 1. Introduction

Azo dyes are an important class of dyes that are widely used in the textile, leather, rubber, paper, and cosmetic industries [1]. After use, azo dyes are generally released into effluents. Their presence in wastewaters causes serious problems for the environment and living organisms, because they are highly resistant to degradation, carcinogenic due to the presence of aryl amines, and persistent in the environment for an extended period of time [2]. A variety of techniques are available nowadays for treating these contaminants. Among these may be mentioned advanced oxidation [3], ozonation [4], biological treatment [5], membrane separation [6], and precipitation [7]. Advanced oxidation processes are considered to be high-cost methods. Biodegradation suffers from optimization problems in addition to the relatively biorefractory character of these dyes. The membrane processes require their

frequent change, while precipitation produces a large amount of sludge and is not suitable for removing low concentrations. Adsorption is especially attractive because of its high efficiency, simplicity of design, and ease of operation [8].

The aim of the study is to examine the ability of modified halloysites for removing RC from synthetic solutions. Three halloysitic solids were used, viz. unmodified halloysite (H), the form calcined at 600 °C (H600), and that processed at 600 °C and with 5N HCl (H600-5N). After characterization, the adsorption of RC was studied by taking into account the effects of kinetics and temperature. A particular interest has been focused on the FTIR study, before and after adsorption. The objective is to understand the uptake mechanism of Congo red.

### 2. Materials and methods

## 2.1 Materials

Halloysite used in this work is from Djebel Debbagh (Algeria). Its characteristics were reported in a previous work [9]. A certain amount of the starting material was heated at 600 °C for 2 h in air atmosphere. Thereafter, 45 g of H600 was mixed with 1125 mL of HCl solution 5N. The suspension was stirred at 70 °C for 4 h then filtered. The recovered solid was abundantly washed with distilled water and dried at 110 °C for 2 h.

## 2.2 Characterization

Chemical analysis and the SiO<sub>2</sub>/Al<sub>2</sub>O<sub>3</sub> molar ratio of the halloysitic solids were determined by ICP-AES on a Perkin-Elmer instrument. TEM images were performed on a JEOL 2100 electron microscope. An EDX detector for X-ray energy dispersive analysis was attached to this microscope. Infrared spectra were recorded with a Shimadzu 1240 FT-IR spectrometer (resolution 2 cm<sup>-1</sup>). The 4000–400 cm<sup>-1</sup> region was studied.

## 2.3 Adsorption procedure

A stock solution of Congo red (CAS No: 573-58-0, chemical formula : C<sub>32</sub>H<sub>22</sub>N<sub>6</sub>Na<sub>2</sub>O<sub>6</sub>S<sub>2</sub>, FW: 696.67 g mol<sup>-1</sup>, λ<sub>max</sub>= 498 nm, supplier : Biochem Chemopharma) of concentration 80 mg L<sup>-1</sup> was prepared. The experiments were performed via the batch method. 0.02 g of halloysitic solid was mixed with 20 mL of aqueous CR solution. pH of the dispersions was adjusted to 6. After each experiment, the solution was separated by centrifugation, then the supernatant was analyzed by visible spectrophotometry at 498 nm, using a Shimadzu 1240 UV-Vis spectrophotometer. The adsorbed amount was calculated from the difference between the initial and final concentrations. The effects of contact time and temperature were studied.

## 2.4 Theoretical considerations

In order to investigate the mechanism controlling adsorption, different equations were applied to model the kinetics of Congo red adsorption onto our materials.

Lagergren [10] proposed a pseudo-first order kinetic model. Its integral form is

$$\log(Q_e - Q_t) = \log Q_e - \frac{K_1 t}{2.303} \quad (1)$$

where  $Q_t$  is the amount adsorbed at time  $t$  (mg/g),  $Q_e$ , the adsorption capacity at equilibrium (mg/g),  $K_1$ ,

the pseudo-first order rate constant (min<sup>-1</sup>), and  $t$  is the contact time (min).

Kinetics may also be described by a pseudo-second order reaction. Its linearized-integral form is [11]:

$$\frac{t}{Q_t} = \frac{1}{K_2 Q_e^2} + \frac{t}{Q_e} \quad (2)$$

where  $K_2$  (g mg<sup>-1</sup> min<sup>-1</sup>) is the pseudo-second order rate constant. The initial rate,  $h$ , as  $t \rightarrow 0$  can be defined as

$$h = K_2 \cdot Q_e^2 \quad (3)$$

The plot of  $t/Q_t$  vs.  $t$  should give a linear relationship, from which  $K_2$  and  $h$  can be determined from the slope and the intercept of the plot.

During adsorption under batch mode, there is a possibility of transport of adsorbate species into the pores of adsorbent, which is often the rate controlling step. The intraparticle diffusion rate equation can be written as follows [12]:

$$Q_t = K_{id} t^{1/2} + C \quad (4)$$

where  $K_{id}$  (mg g<sup>-1</sup> min<sup>-1/2</sup>) is the intraparticle diffusion rate constant and  $C$ , a constant. The  $K_{id}$  and  $C$  values are calculated from the slope and the intercept of the plot of  $Q_t$  versus  $t^{1/2}$ , respectively.

## 2.5 Thermodynamic study

The parameters  $\Delta H^0$ ,  $\Delta S^0$ , and  $\Delta G^0$  were evaluated using the following equation

$$\ln K_d = \frac{-\Delta H^0}{R.T} + \frac{\Delta S^0}{R} \quad (5)$$

where  $\Delta H^0$  (kJ mole<sup>-1</sup>) and  $\Delta S^0$  (J mole<sup>-1</sup> K<sup>-1</sup>) are enthalpy and entropy changes, respectively;  $T$  (K), absolute temperature;  $R$  (J mol<sup>-1</sup> K<sup>-1</sup>), gas constant;  $K_d$  (L g<sup>-1</sup>), distribution coefficient, which is given by

$$K_d = \frac{Q_e}{C_e} \quad (6)$$

Enthalpy and entropy changes are graphically determined by plotting  $\ln K_d$  versus  $1/T$ , which gives a straight line. According to thermodynamics, the Gibbs free energy change,  $\Delta G^0$ , is related to  $\Delta H^0$  and  $\Delta S^0$  by the following equation

$$\Delta G = \Delta H^0 - T\Delta S^0 \quad (7)$$

Table 1. Chemical composition of raw and modified halloysite

Samples	SiO <sub>2</sub> (%)	Al <sub>2</sub> O <sub>3</sub> (%)	CaO (%)	Fe <sub>2</sub> O <sub>3</sub> (%)	K <sub>2</sub> O (%)	MgO (%)	MnO (%)	Na <sub>2</sub> O (%)	Molar ratio SiO <sub>2</sub> /Al <sub>2</sub> O <sub>3</sub>
H	49.1	46.16	0.94	1.25	0.31	0.21	1.44	0.54	1.81
H600	44.7	39.69	0.65	0.45	0.32	0.05	2.01	0.34	1.92
H600-5N	73.0	4.59	0.03	0.09	0.30	0.003	0.05	0.16	27.11

### 3. Results and discussion

#### 3.1 Characterization

##### 3.1.1. Chemical Analysis

Chemical compositions of the halloysitic solids are presented in Table 1. Raw halloysite (H) contains alumina and silica in major quantities, contrary to other oxides. When halloysite is treated at 600 °C (H600), its SiO<sub>2</sub>/Al<sub>2</sub>O<sub>3</sub> molar ratio increases slightly from 1.81 to 1.92, consequence of the dehydroxylation of structural aluminol groups [13]. After thermochemical modification, the chemical composition of H600-5N changes profoundly. Molar ratio increases up to 27.11, while the percentage of Fe<sub>2</sub>O<sub>3</sub>, CaO, MgO, and MnO diminishes considerably. The decrease in alumina content can be ascribed to the leaching of the Al<sup>3+</sup> ions from the octahedral sheet [14]. Acid attack also leads to the elimination of a great part of impurities [15].

##### 3.1.2. Transmission electron microscopy

TEM images of H600 and H600-5N are presented in Fig 1. H600 highlights particles having a cylindrical shape and containing a transparent central area that runs longitudinally along the cylinder. The nanotubular particles obtained are hollow and open-ended. Their size is different both in diameter and length. Their external and internal diameters vary from 30 to 180 nm and from 10 to 30 nm, respectively. These rolled tubes consist in a number of aluminosilicate layers curved and closely packed. This morphology was also obtained for the unmodified halloysite [16], proving that the thermal treatment at 600 °C conserves the tubular nature of the Algerian halloysite. A phase rich in Mn, Al, and O was evidenced by EDX in microscope. This phase consists in agglomerated small plates of diameter 10 nm. Interlayer spacing could not be highlighted. This is probably due to the fact that the layers are immediately destroyed under the beam of electrons.

The sample H600-5N (Fig.1) also leads to a tubular morphology, although the tubes obtained are

somewhat damaged. Dehydroxylation associated with the leaching of Al<sup>3+</sup> alter slightly the nanotubes. The observation of the morphological details is of a great relevance. The defects on the surface such as surface breakage or crystallographic defects could prove as potential reaction sites for the surface chemistry of halloysitic clays.

#### 3.2 Congo red adsorption

##### 3.2.1. Kinetics

The effect of contact time is reported in Fig.2. Adsorption rate is rapid in the first 10 min, then it decreases continuously, reaching equilibrium at about 2 h. So, an agitation time of 2 h seems to be sufficient for equilibrium experiments. Fast initial adsorption could be attributed to the presence of a great number of vacant sites and a high gradient of solute concentrations [17]. Highest capacity in CR adsorption was found for H600-5N.

The parameters of the kinetic models used are presented in Table 2. The pseudo-first order equation does not apply, because the estimated theoretical quantities,  $Q_e$  (cal), are different from the experimental values,  $Q_e$  (exp). Also, the curves diverge from linearity (Fig.3). The fit of the experimental data with the pseudo-second order model is more suitable.

Linear plots of  $t/Q_t$  vs.  $t$  (Eq.(2)) were obtained (Fig.4), corresponding to high  $R^2$  values, i.e.,  $\geq 0.99$ , while the  $Q_e$  (cal) values are closely linked to those of  $Q_e$  (exp).

The use of the intraparticle diffusion model requires the plotting  $Q_t$  against  $t^{1/2}$  (Fig.5). This model is not the only rate-controlling step, due to the deviation of the plots from the origin ( $C$  values  $\neq 0$ , Table 2).

As consequence, the boundary layer diffusion affects the CR adsorption to some extents. The values of intercept,  $C$ , give an idea about the thickness of boundary layer, i.e., the larger the intercept, the greater is the boundary layer effect [18]. The  $C$  values of H600-5N rise considerably compared to those of the unmodified halloysite. At 55 °C, it is 3.32 times larger than that of H.

Treatment with HCl disrupts the interfacial properties of halloysitic clay, so the effect of boundary layer plays a prominent role.

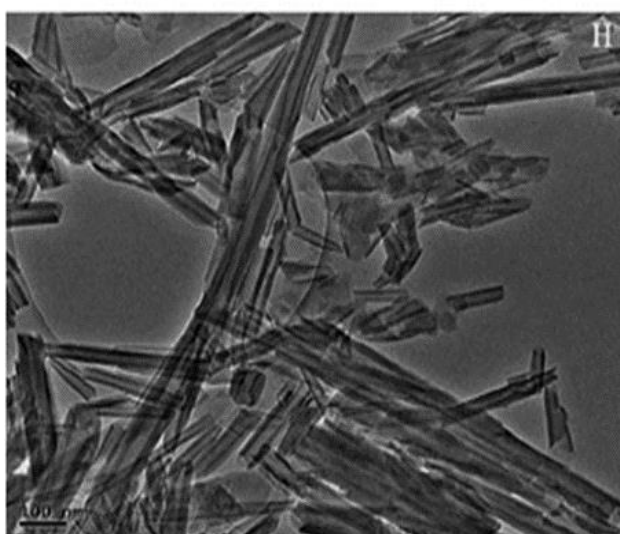
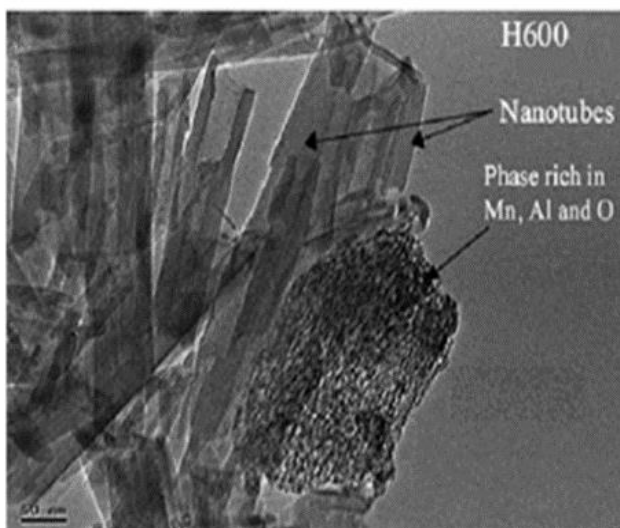
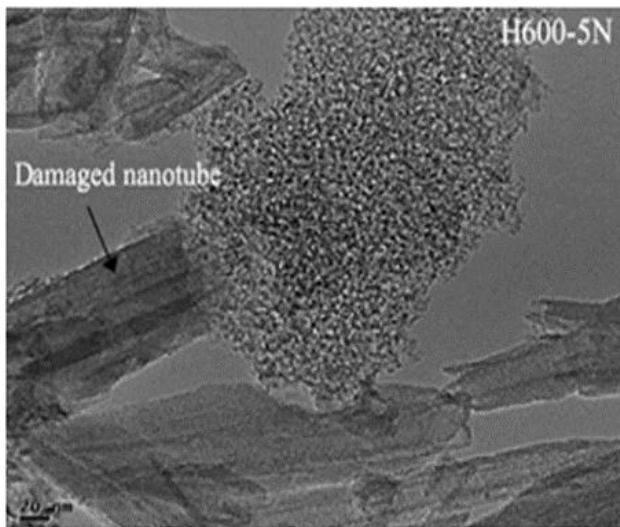


Figure.1 Transmission electron microscopy images of H, H600, and H600-5N.

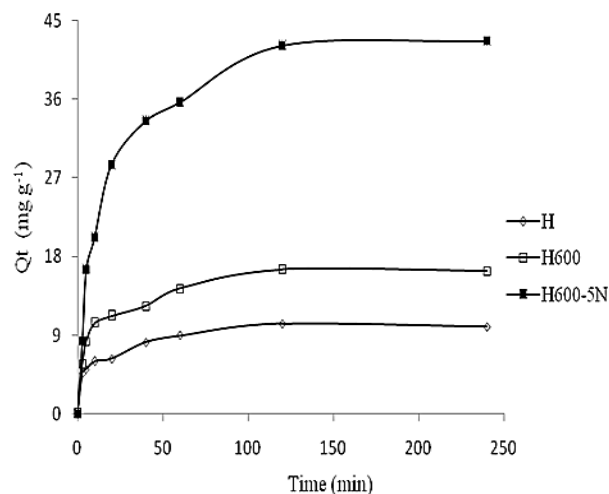


Figure.2 Effect of contact time on the uptake CR of H, H600 and H600-5N, at 55 °C

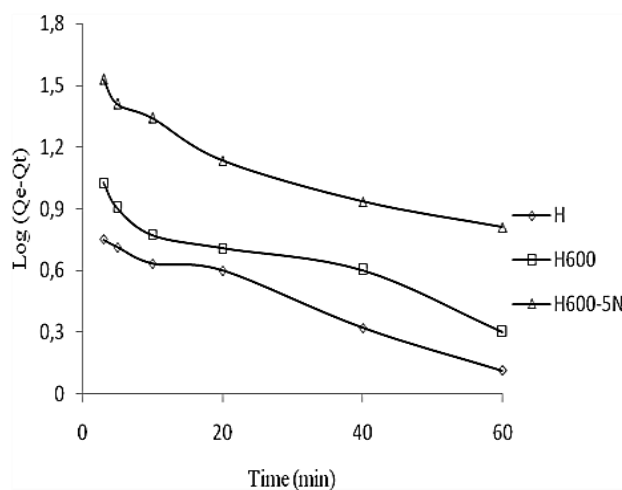


Figure.3 Pseudo first order kinetic for the adsorption of CR onto halloysitic solids

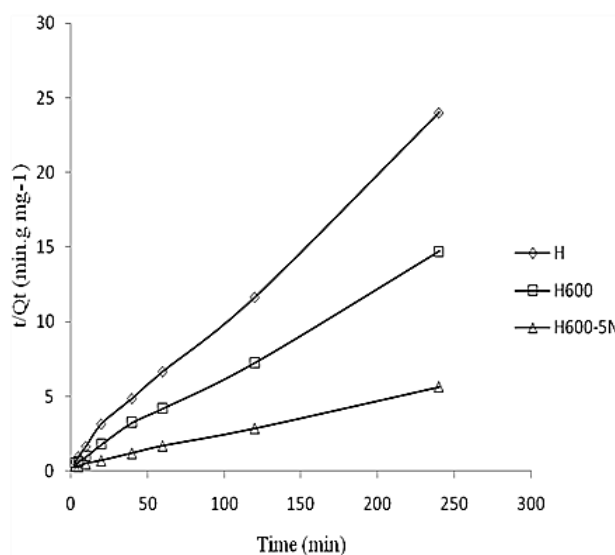


Figure.4 Pseudo second order kinetic for the adsorption of CR onto halloysitic solids

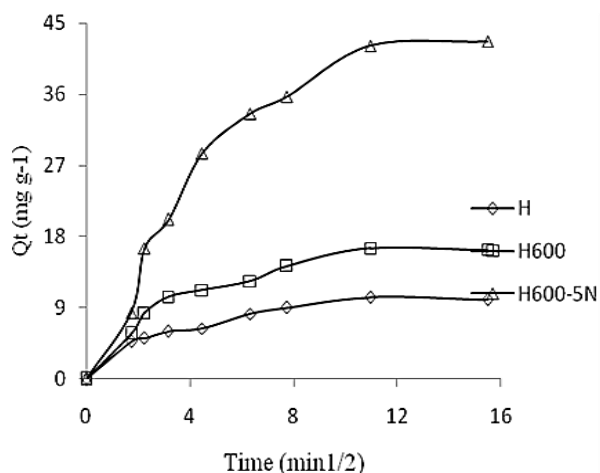


Figure 5. Intraparticle diffusion effect on the adsorption of CR ion onto halloysitic solids

### 3.2.2. Thermodynamics

The values of free energy ( $\Delta G^\circ$ ), enthalpy ( $\Delta H^\circ$ ), and entropy ( $\Delta S^\circ$ ) are listed in Table 3. The  $\Delta G^\circ$  values are positive in the temperature range studied, revealing a process not spontaneous with possibility of chemisorption [19]. These values decrease with increasing temperature regardless of the material, indicating that better adsorption is obtained at higher temperatures. The positive  $\Delta H^\circ$  values highlight the endothermic character of CR adsorption. The process is, thus, favored by an increase in temperature via the activation of the adsorption sites [20]. The positive entropies suggest an increase in randomness at the solid–solution interface, for which significant changes occur in the internal structure of the adsorbents, after adsorption. [21].

### 3.2.3. FTIR analysis

The infrared spectra of H, H600-5N, CR, and CR-loaded H600-5N (H600-5N after adsorption of Congo red), were recorded in the 4000–400  $\text{cm}^{-1}$  range and depicted in (Fig.6).

The FTIR spectrum of the starting material (Fig 6–H) shows two bands at 3704 and 3632  $\text{cm}^{-1}$  attributed to the stretching vibrations of the inner surface and inner sheet hydroxyls, respectively [22]. The band at 3436  $\text{cm}^{-1}$  indicates the stretch of interlayer water. The 1626  $\text{cm}^{-1}$  band represents the hydration of  $\delta\text{AlOH}$  [23]. The 1081  $\text{cm}^{-1}$  band is assigned to the stretching mode of apical Si–O, whilst those at 1042 and 922  $\text{cm}^{-1}$  are caused by the stretch of Si–O–Si and the bending of Al–O–H, respectively [24]. The bands at 548 and 484  $\text{cm}^{-1}$  are attributed to Al–O–Si and Si–O–Si bendings, respectively.

Significant changes occur in the vibrational spectrum when halloysite was heat-treated and acid-

leached (Fig 6–H600-5N). The broadening of the 3429  $\text{cm}^{-1}$  band reveals the formation of silica nanoparticles [25]. The persistence of 1622  $\text{cm}^{-1}$  band may be assigned to the hydration of  $\delta\text{SiOH}$  instead of AlOH, given the elimination of Al by acid attack. The abatement of the stretch at 1081  $\text{cm}^{-1}$ , the widening of the 1077  $\text{cm}^{-1}$  band, the disappearance of the vibrations at 760 (Si–O–Al perpendicular stretching) and 682  $\text{cm}^{-1}$  (Si–O–Al), the decrease in the band at 527  $\text{cm}^{-1}$ , show the formation of amorphous silica [26] and the elimination of aluminium from octahedral sheets [25]. This interpretation is in conformity with the evolution of  $\text{SiO}_2/\text{Al}_2\text{O}_3$  molar ratio, which increases from 2.08 (H) to 27.11 (H600-5N) (Table 1).

The spectrum of Congo red before adsorption (Fig.6 –CR) exhibits bands at 3470 and 3384  $\text{cm}^{-1}$  due to the asymmetrical and symmetrical N–H stretches of primary amines, respectively [27]. The 3181  $\text{cm}^{-1}$  band is associated with C–H vibrations in aromatic rings. The N–H bending of primary amine occurs at 1630  $\text{cm}^{-1}$ . The band at 1451  $\text{cm}^{-1}$  is indicative of the vibration of C=C bonds in the aromatic ring. The asymmetric and symmetric vibrations of S=O in sulfonate groups appear at 1172 and 1059  $\text{cm}^{-1}$ , respectively. Medium bands arise in the 900–650  $\text{cm}^{-1}$  range, indicating N–H wagging, while that at 534  $\text{cm}^{-1}$  is due to torsional N–H oscillation.

The results of H600-5N after exposure to a solution of 400  $\text{mg L}^{-1}$  of CR (Fig.6 –CR-loaded H600-5N) highlight some modifications of the absorption bands: some vanish while others are found to shift. The 3432 and 1631  $\text{cm}^{-1}$  bands decrease in intensity and shift slightly after CR adsorption, denoting a deep involvement of amino groups [27]. The same behavior was obtained for the bands at 1172 and 1059  $\text{cm}^{-1}$  (asymmetric and symmetric vibrations of S=O), which indicates the implication of sulfonate anions via S=O groups. The shift of 1622 band towards 1635  $\text{cm}^{-1}$  and the decrease of its intensity prove that RC molecules interact with SiOH( $\text{H}_2\text{O}$ ) species.

Goynes et al. [28] showed that the proton dissociation on silanol surface sites starts at circumneutral pH. Bearing in mind that adsorption was performed at pH 6, the interaction of AH600-5N occurs via SiOH groups. The latter are bound to  $\text{H}_2\text{O}$  via H-bonds, forming SiOH... $\text{H}_2\text{O}$  species [29]. On the basis of the spectroscopic study, the mechanism is an outer-sphere surface complexation of SiOH... $\text{H}_2\text{O}$  (H600-5N) by Congo red molecules via amine ( $\text{NH}_2$ ) and sulfoxide (S=O) groups, which provide the nonbonding electrons from nitrogen and sulfur atoms, respectively.

Table 2. Kinetic parameters for CR adsorption onto modified halloysites

Samples	T (°C)	Q <sub>t</sub> (exp) (mg g <sup>-1</sup> )	Pseudo-first order model			Pseudo-second order model				Intraparticle diffusion model		
			Q <sub>t</sub> (cal) (mg g <sup>-1</sup> )	K <sub>1</sub> (min <sup>-1</sup> )	R <sup>2</sup>	Q <sub>t</sub> (cal) (mg g <sup>-1</sup> )	K <sub>2</sub> (g mg <sup>-1</sup> min <sup>-1</sup> )	h (mg g <sup>-1</sup> min <sup>-1</sup> )	R <sup>2</sup>	K <sub>id</sub> (mg g <sup>-1</sup> min <sup>-1/2</sup> )	C (mg g <sup>-1</sup> )	R <sup>2</sup>
H	25	21.05	16.71	0.037	0.991	22.22	0.0042	2.09	0.999	2.54	0.97	0.979
	40	28.32	23.60	0.025	0.975	32.26	0.0016	1.69	0.998	3.22	1.06	0.999
	55	10.30	5.96	0.025	0.989	10.42	0.0013	1.41	0.997	0.72	3.52	0.952
H600	25	32.28	26.92	0.035	0.984	34.48	0.0021	2.48	0.998	3.11	5.46	0.969
	40	25.65	18.45	0.035	0.976	27.07	0.0039	2.87	0.998	2.04	7.11	0.985
	55	16.54	9.27	0.023	0.926	16.95	0.0072	2.07	0.997	0.83	7.58	0.955
H600-5N	25	25.43	16.48	0.014	0.781	27.78	0.0022	1.68	0.990	0.90	9.95	0.999
	40	38.02	28.12	0.021	0.977	41.67	0.0015	2.60	0.995	2.80	10.16	0.996
	55	42.12	29.51	0.028	0.937	45.45	0.0018	3.76	0.999	3.27	11.70	0.919

Table 3. Thermodynamic parameters for the CR adsorption onto modified halloysites

Samples	ΔH (kJ mole <sup>-1</sup> )	ΔS (kJ mole K <sup>-1</sup> )	ΔG (kJ mole <sup>-1</sup> )		
			25 °C	40 °C	55 °C
H	8.31	0.010	5.22	5.07	4.91
H600	12.69	0.025	5.22	4.85	4.47
H600-5N	12.67	0.028	4.44	4.03	3.61

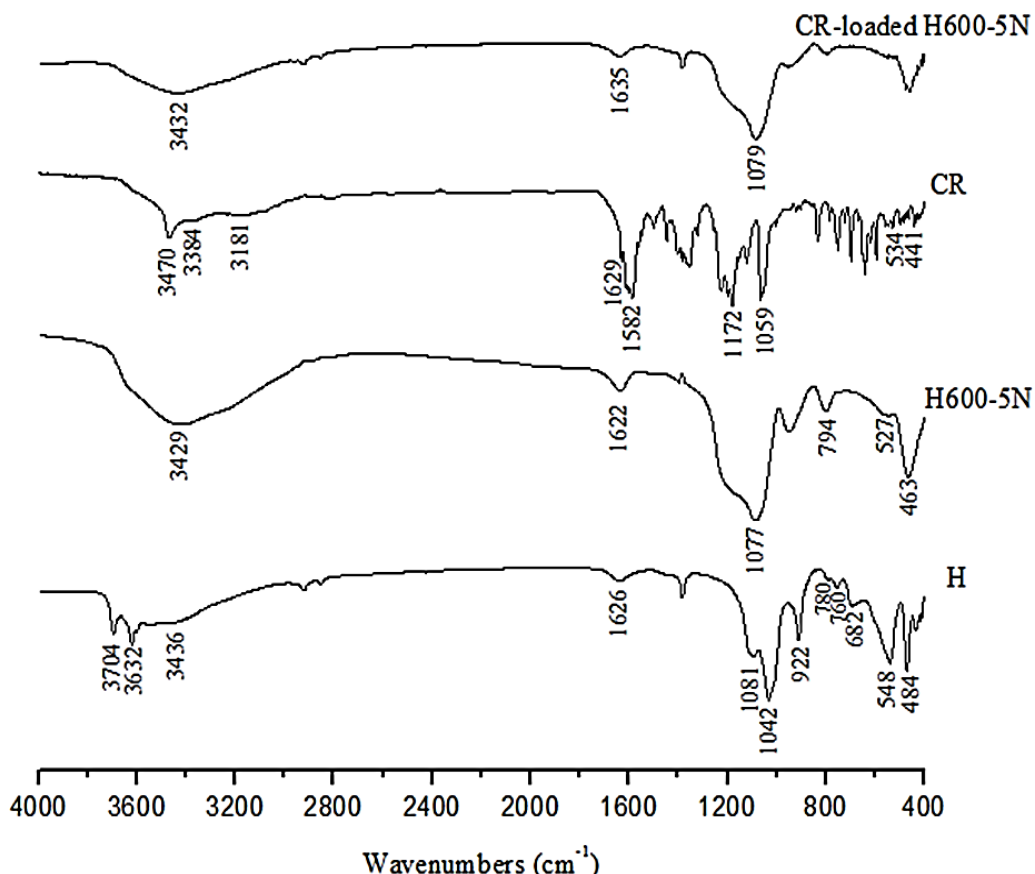


Figure.6 FTIR spectra of H, H600-5N, CR, and CR-loaded H600-5N

#### 4. Conclusion

Thermo-chemical modification of halloysite at 600 °C and with HCl 5N leads to dehydroxylation of

the structure and the leaching of Al ions from octahedral sheet. As consequence, SiO<sub>2</sub>/Al<sub>2</sub>O<sub>3</sub> molar ratio increases from 1.81 to 27.11. This treatment maintains the tubular nature of our halloysite. The kinetics of Congo red adsorption

follows the pseudo second order model with a contribution of intraparticle diffusion. Thermodynamic parameters highlight a not spontaneous and endothermic character. Spectroscopic study shows an outer-sphere surface complexation between SiOH...H<sub>2</sub>O and nonbonding electrons of nitrogen and sulfur atoms of amine (NH<sub>2</sub>) and sulfoxide (S=O) groups, respectively.

In this study, only a monosolute system was investigated and few research on multisolute systems have been reported. In practice, most industrial effluents contain a mixture of dyes. Therefore, it is necessary to study the simultaneous removal of two or several dyes from aqueous solutions, even from industrial discharges.

## References

- [1] S. Dawood and T.K. Sen, "Removal of anionic dye Congo red from aqueous solution by raw pine and acid-treated pine cone powder as adsorbent, equilibrium, thermodynamic, kinetics, mechanism and process design", *Water, Res.*, Vol. 46, pp.1933–1946, 2012.
- [2] A.R. Gregory, S. Elliot, and P. Kluge, "Ames testing of direct black 3B parallel carcinogenicity", *Journal of Applied Toxicology*, Vol. 1, No.6, pp.308-313, 1991.
- [3] W. Chen, L. Wangyang, Y. Yao, and M. Xu, "Highly efficient decomposition of organic dyes by aqueous-fiber phase transfer and in situ catalytic oxidation using fiber-supported cobalt phthalocyanine", *Environ. Sci. Technol.*, Vol. 41, No.17, pp. 6240–6245, 2007.
- [4] X. Zhang, W. Dong, F. Sun, W. Yang, and J. Dong, "Degradation efficiency and mechanism of azo dye RR2 by a novel ozone aerated, internal microelectrolysis filter", *J. Hazard. Mater.*, Vol. 276, pp. 77–87, 2014.
- [5] D. Cui, Y.Q. Guo, H.S. Lee, H.Y. Cheng, B. Liang, F.Y. Kong, Y.Z. Wang, L.P. Huang, M.Y. Xu, and A. J. Wang, "Efficient azo dye removal in bioelectrochemical system and post-aerobic bioreactor: optimization and characterization", *Chem. Eng. J.*, Vol. 243, pp. 355–363, 2014.
- [6] S. Cheng, D.L. Oatley, P.M. Williams, and C.J. Wright, "Characterisation and application of a novel positively charged nanofiltration membrane for the treatment of textile industry wastewaters", *Water Res.*, Vol. 46, pp.33–42, 2012.
- [7] B. Ismail, S.T. Hussain, and S. Akram, "Adsorption of methylene blue onto spinel magnesium aluminate nanoparticles: adsorption isotherms, kinetic and thermodynamic studies", *Chem. Eng. J.*, Vol. 219, pp.395–402, 2013.
- [8] A. Gurses, C. Dogar, M. Yalcin, M. Acikyildiz, R. Bayrak, and S. Karaca, "The adsorption kinetics of the cationic dye, methylene blue, onto clay", *J. Hazard. Mater.*, Vol. 131, pp. 217–228, 2006.
- [9] S. Mellouk, S. Cherifi, M. Sassi, K. Marouf-Khelifa, A. Bengueddach, J. Schott, and A. Khelifa, "Intercalation of halloysite from Djebel Debagh (Algeria) and adsorption of copper ions", *Appl. Clay Sci.*, Vol. 44, pp. 230–236, 2009.
- [10] S. Lagergren, "Zur theorie der sogenannten adsorption geloster stoffe (About the theory of so-called adsorption of soluble substances), Kungliga Svenska Vetenskapsademiens, Handlingar", *K. Sven. Vetenskapsakad. Handl.*, Vol. 24, pp.1–39, 1898.
- [11] Y.S. Ho and G. McKay, "Pseudo-second order model for sorption processes", *Process Biochem*, Vol. 34, pp. 451–465, 1999.
- [12] W.J. Weber and J.C. Morris, "Kinetics of adsorption on carbon from solution", *J. Sanitary Eng. Div. Am. Soc. Civ. Eng.*, Vol.89, pp.31–59, 1963.
- [13] P. Yuan, P.D. Southon, Z. Liu, M.E.R. Green, J.M. Hook, S.J. Antill, and C.J. Kepert, "Functionalization of halloysite clay nanotubes by grafting with  $\gamma$ -aminopropyltriethoxysilane", *Phys. Chem. C*, Vol. 112, pp.15742–15751, 2008.
- [14] A.K. Panda, B.G. Mishra, D.K. Mishra, and R.K. Singh, "Effect of sulphuric acid treatment on the physico-chemical characteristics of kaolin clay", *Colloids and Surfaces A*, Vol.363, pp.98–104, 2010.
- [15] J.D.D. Melo, T.C.C. Costa, A.M. Medeiros, and C.A. Paskocimas, "Effects of thermal and chemical treatments on physical properties of kaolinite", *Ceramics International*, Vol.36, pp.33–38, 2010.
- [16] F. Bessaha, K. Marouf-Khelifa, I. Batonneau-Gener, and A. Khelifa, "Characterization and application of heat-treated and acid-leached halloysites in the removal of malachite green: adsorption, desorption, and regeneration studies", *Des. Water. Treat.*, Vol.57, pp.14609–14621, 2016.
- [17] L. Zhang, H. Zhang, W. Guo, and Y. Tian, "Removal of malachite green and crystal violet cationic dyes from aqueous solution using activated sintering process red mud", *Appl. Clay. Sci.*, Vol.93, pp.85–93, 2014.

- [18] N.K. Kannan and M.M. Sundaram, "Kinetics and mechanism of removal of methylene blue by adsorption on various carbons- A comparative study", *Dyes Pigm.*, Vol.51, pp. 25–40, 2001.
- [19] Y. Salameh, N. Al-Lagtah, M.N.M. Ahmad, S.J Allen, and G.M. Walker, "Kinetic and thermodynamic investigations on arsenic adsorption onto dolomitic sorbents", *Chem. Eng. J.* Vol.160, pp.440-446, 2010.
- [20] K. Vijayaraghavan and Y.S. Yun, "Biosorption of C.I. Reactive Black 5 from aqueous solution using acid-treated biomass of brown seaweed *Laminaria* sp", *Dyes and Pigments*, Vol.76, pp. 726–732, 2008.
- [21] M. Alkan, O. Demirbas, and M. Dogan, "Adsorption kinetics and thermodynamics of an anionic dye onto sepiolite", *Microporous Mesoporous Mater.*, Vol.101, pp.388–396, 2007.
- [22] N. Mahrez, S. Bendenia, K. Marouf-Khelifa, I. Batonneau-Gener, and A. Khelifa, "Improving of the adsorption capacity of halloysite nanotubes intercalated with dimethyl sulfoxide", *J. Composite Interfaces*, Vol.22, pp.403-417, 2015.
- [23] E. Srasra, F. Bergaya, and J.J. Fripiat, "Infrared spectroscopy study of tetrahedral and octahedral substitutions in an interstratified illite-smectite", *Clay clays and clay minerals*, Vol.42, pp.237–241, 1994.
- [24] Y. Deng, G.N. White and J.B. Dixon, "Effect of structural stress on the intercalation rate of kaolinite", *J. Colloid Interface Sci.*, Vol.250, pp.379–393, 2002.
- [25] E. Abdullayev, A. Joshi, W. Wei, Y. Zhao, and Y. Lvov, "Enlargement of halloysite clay nanotube lumen by selective etching of aluminum oxide", *ACS Nano*, Vol.6, pp.7216–7226, 2012.
- [26] J.P. Nguetnkam, R. Kamga, F. Villieras, G.E. Ekodeck, A. Razafitianamaharavo, and J. Yvon, "Assessment of the surface areas of silica and clay in acid-leached clay materials using concepts of adsorption on heterogeneous surfaces", *J. Colloid Interface Sci.*, Vol.289, pp.104–115, 2005.
- [27] R.M. Silverstein, G.C. Bassler, and T.C. Morrill, "Spectrometric Identification of the Organic Compounds, fifth ed", *De Boeck Universite', Bruxelles*, 1998. (in French).
- [28] K.W. Goyne, "Surface Charge of Variable Porosity  $\text{Al}_2\text{O}_3(\text{s})$  and  $\text{SiO}_2(\text{s})$  Adsorbents", *J. Porous Mater.*, Vol.9, pp.243–256, 2002.
- [29] L.T. Zhuravlev, "The surface chemistry of amorphous silica. Zhuravlev model", *Colloids and Surf A*, Vol.173, pp.1–38, 2000.